Supporting information

FeSb/FeS heterostructures anchored on exfoliated graphite nanosheets as an advanced anode for sodium-ion batteries

Ting Yue[a], Liwen Zhang[a], Shandong Huang[a], Lichen Zhang[a], Xintong Wang[a], Huile Jin[a], Yihong Ding[a]*, Tianbiao Zeng[b]*

[a]. Key Laboratory of Carbon Materials of Zhejiang Province, Wenzhou Key Lab of Advanced Energy Storage and Conversion, Zhejiang Province Key Lab of Leather Engineering, College of Chemistry and Materials Engineering, Wenzhou University, Wenzhou, Zhejiang 325035, China

[b]. Research Institute of Interdisciplinary Sciences (RISE) and School of Materials Science & Engineering, Dongguan University of Technology, Dongguan 523808, China

*: Corresponding author: yhdd@wzu.edu.cn (Y. Ding), tianbiaoZeng@126.com (T. Zeng).

Text 1

Considering that Fe is an abundant resource in nature, Fe was selected as the reductant to react with Sb_2S_3. It should be noted that Fe is a Na-inert element and the introduction of Fe into the electrode system reduces the theoretical capacity. The theoretical capacity of Sb_2S_3 is 946 mAh/g. The reaction equation for the preparation of FeSb/FeS from 5:1 Fe/Sb_2S_3 powder is:

$$5Fe + Sb_2S_3 = 2FeSb + 3FeS \tag{1}$$

The theoretical capacity of FeSb/FeS can be calculated according to the following equation:

$$C_{FeSb/FeS} = \frac{12 \times 96485.6}{3.6 \times (55.845 \times 5 + 339.715)} = 519.628\ mAh/g \tag{2}$$

In equation (2), the Faraday constant is 96485.6 C/mol, each mole of Sb_2S_3 can accommodate up to 12 moles of sodium ions, 1 mAh = 3.6 C, the molar mass of Fe is 55.845 g/mol, and the molar mass of Sb_2S_3 is 339.715 g/mol. Therefore, the theoretical capacity of FeSb/FeS is: 519.628 mAh/g.

Text 2

The specific equation for calculating the charge density differential is as follows: [1]

$$\Delta\rho = \rho_{AB} - \rho_A - \rho_B \tag{3}$$

Here, ρ_{AB} represents the charge density difference of the system AB, ρ_A represents the charge density difference of the fragments A in the system, and ρ_B represents the charge density difference of the fragments B that in the system.

Text 3

According to the Conway theory by B.E., the surface pseudocapacitance was determined through CV scans performed at scan rates ranging from 0.2 to 1.0 mV/s: [2, 3]

$$i = av^b \tag{4}$$

$$\log i = \log a + b\log v \tag{5}$$

Here, i represents the measured current (mA), v is the voltage sweep rate ($mV\cdot s^{-1}$), and a and b are parameters that vary with scan rate. When $b = 0.5$, the electrode material exhibits diffusion-dominated sodium storage behavior; when the value of b is in the range of 0.5 to 1, the electrode material demonstrates a coexistence of diffusion and pseudocapacitive sodium storage behavior; when $b \geq 1$ the electrode material exhibits pseudocapacitive sodium storage behavior.

$$i = k_1 v + k_2 v^{1/2} \tag{6}$$

$$\frac{i}{v^{\frac{1}{2}}} = k_1 v^{1/2} + k_2 \tag{7}$$

Here, k_1 and k_2 are adjustable constants. $k_1 v$ and $k_2 v^{1/2}$ represent pseudocapacitive control and diffusion control, respectively. The Na^+ diffusion coefficient (D_{Na^+}) is calculated using the following equation: [4, 5]

$$D_{Na^+} = \frac{4}{\pi \cdot \tau} \cdot \left(\frac{m_B \cdot V_m}{M_B \cdot S}\right)^2 \cdot \left(\frac{\Delta E_s}{\Delta E_\tau}\right)^2 \tag{8}$$

Here, τ represents the duration of the current pulse (s), Vm is the molar volume ($cm^3\ mol^{-1}$), m_B is the mass of the active substance (g), M_B is the molar mass of the electrode material ($g\ mol^{-1}$), S is the contact surface area between the electrode and electrolyte (cm^2), and ΔE_s and ΔE_τ represent the potential changes during the pulse and relaxation processes, respectively.

Text 4

In the MD simulations, the crystal structure is constructed based on the standard crystal structure and the kpoint mesh uses only gamma points. The Na^+ diffusion coefficient is calculated according to the following equation: [6, 7]

$$D_{Na^+} = \lim_{t \to \infty} \frac{< r^2(t) >}{6\,dt} \qquad (9)$$

Here, $< r^2(t) >$/**t** is the mean square displacement (MSD) slope of Na diffusion. The work function is calculated by the following equation:

$$E_w = E_v - E_F \qquad (10)$$

Here, E_v is the surface vacuum energy level of the electrons in the particular structure and E_F is the Fermi energy level of the electrons in the said structure.

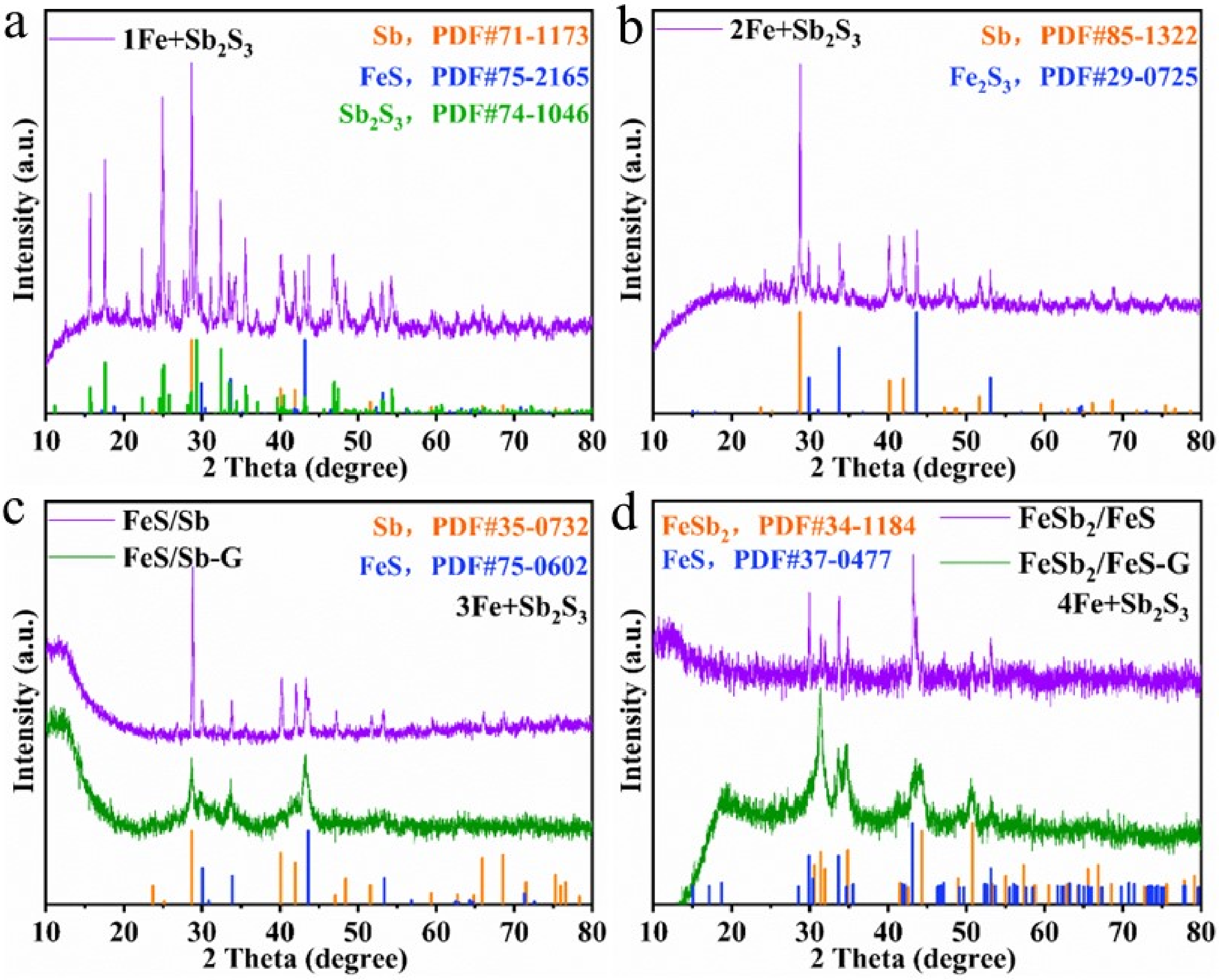

Fig. S1. (a) XRD pattern of the product with a molar ratio of Fe to Sb_2S_3 of 1:1, (b) XRD pattern of the product with a molar ratio of Fe to Sb_2S_3 of 2:1, (c) XRD pattern of the product with a molar ratio of Fe to Sb_2S_3 of 3:1, FeS/Sb product and the ball-milled FeS/Sb-G product, (d) XRD pattern of the product with a molar ratio of Fe to Sb_2S_3 of 4:1, $FeSb_2$/FeS product and the ball-milled $FeSb_2$/FeS-G product.

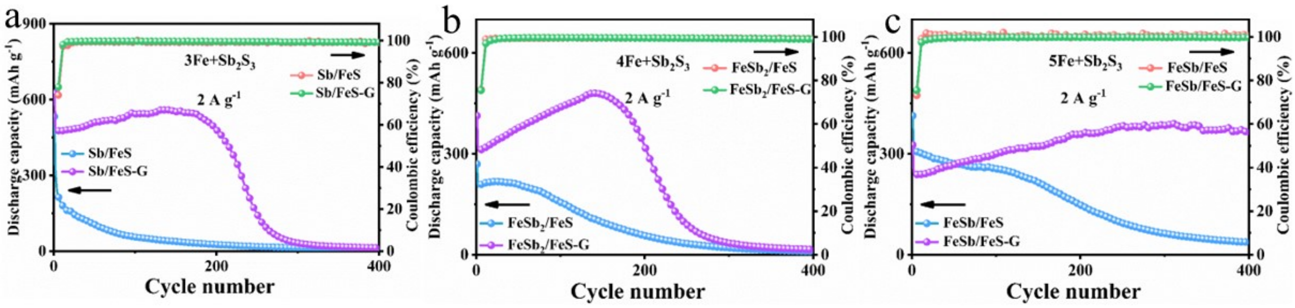

Fig. S2. (a, b, c) show the cycling performance of the products before and after ball milling of Fe and Sb_2S_3 at molar ratios of 3:1, 4:1, and 5:1, respectively, under a current density of 2 A/g.

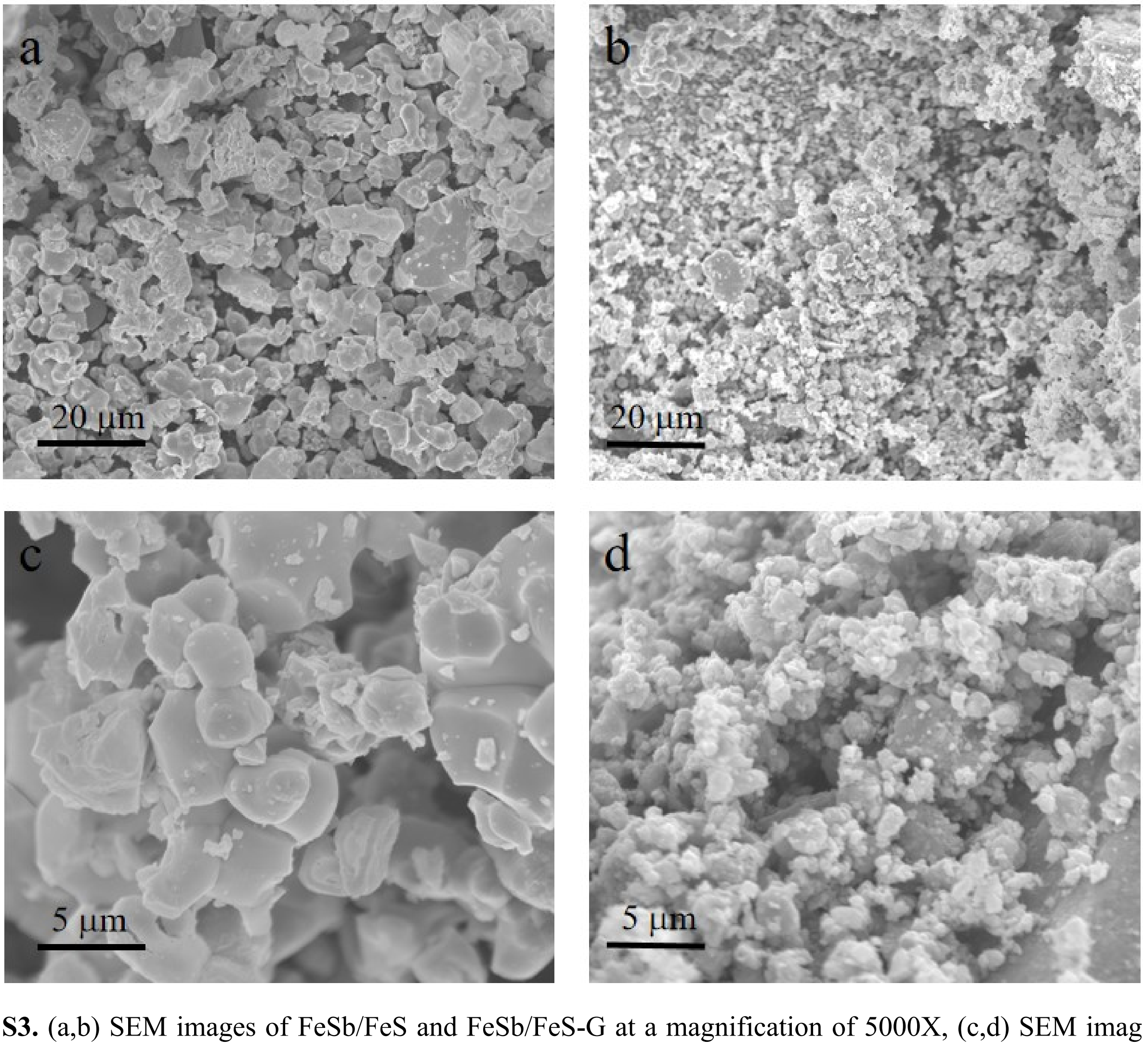

Fig. S3. (a,b) SEM images of FeSb/FeS and FeSb/FeS-G at a magnification of 5000X, (c,d) SEM images of

FeSb/FeS and FeSb/FeS-G at a magnification of 20000X.

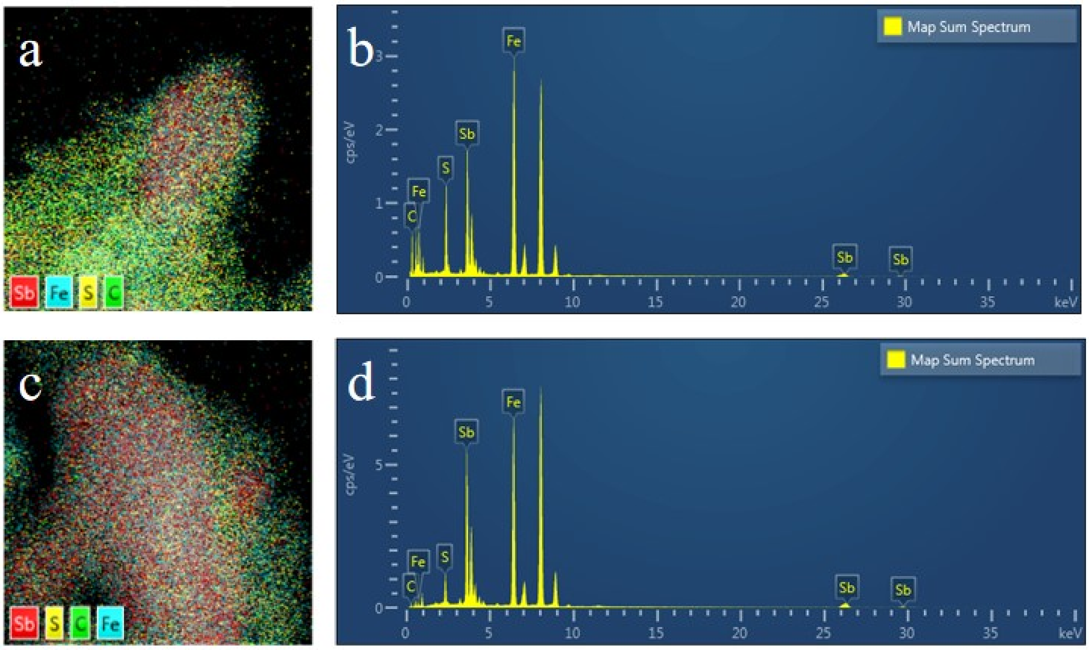

Fig. S4. (a,c) Elemental mapping images of FeSb/FeS-G, (b,d) EDS spectra corresponding to (a) and (c).

Figure S5 presents the *ex*-situ XRD patterns of the FeSb/FeS electrode after five cycles at a current density of 0.2 A/g. The measurements were conducted at various states, including discharge to 0.25 V, discharge to 0 V, discharge to 0 V followed by charge to 1 V, discharge to 0 V followed by charge to 3 V, discharge to 0 V followed by charge to 3 V then discharge to 0.75 V, discharge to 0 V followed by charge to 3 V then discharge to 0 V, discharge to 0 V→ charge to 3 V → discharge to 0 V → charge to 1 V, and discharge to 0 V →charge to 3 V → discharge to 0 V → charge to 3 V. The results show that the characteristic peaks of Cu and FeSb are consistently observed throughout the charge/discharge process, indicating the partial reversibility of FeSb.

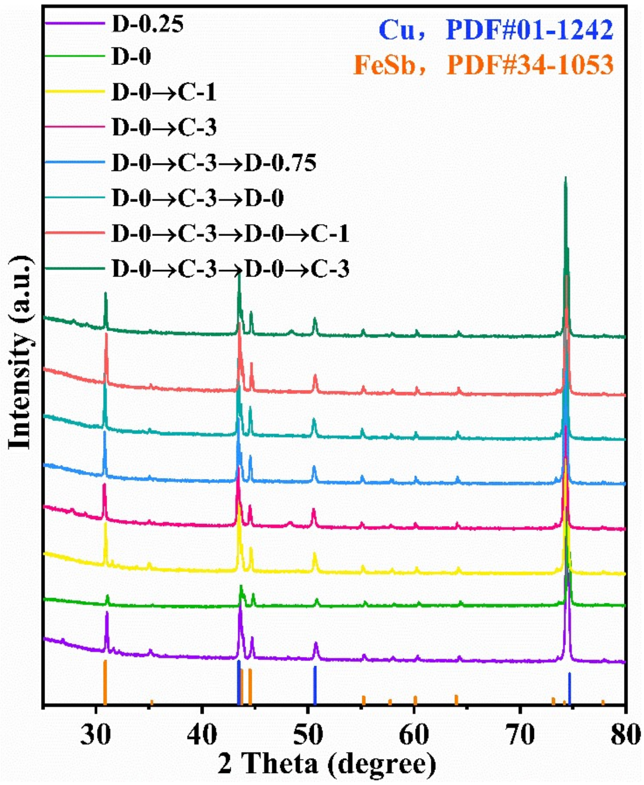

Fig. S5. *Ex*-situ XRD patterns of FeSb/FeS during the discharge/charge processes.

After 100 stable cycles at a current density of 6 A/g, *ex*-situ XPS measurements were conducted on the FeSb/FeS-G electrode at discharged (0 V) and charged (3 V) states. The spectra at the fully charged state (3 V) exhibit two Sb–Sb peaks, identical to those of the pristine electrode. However, after discharge to 0 V, an additional peak at 535.6 eV corresponding to Na–Sb bonding was observed, which was attributed to the formation of Na_3Sb.[8]

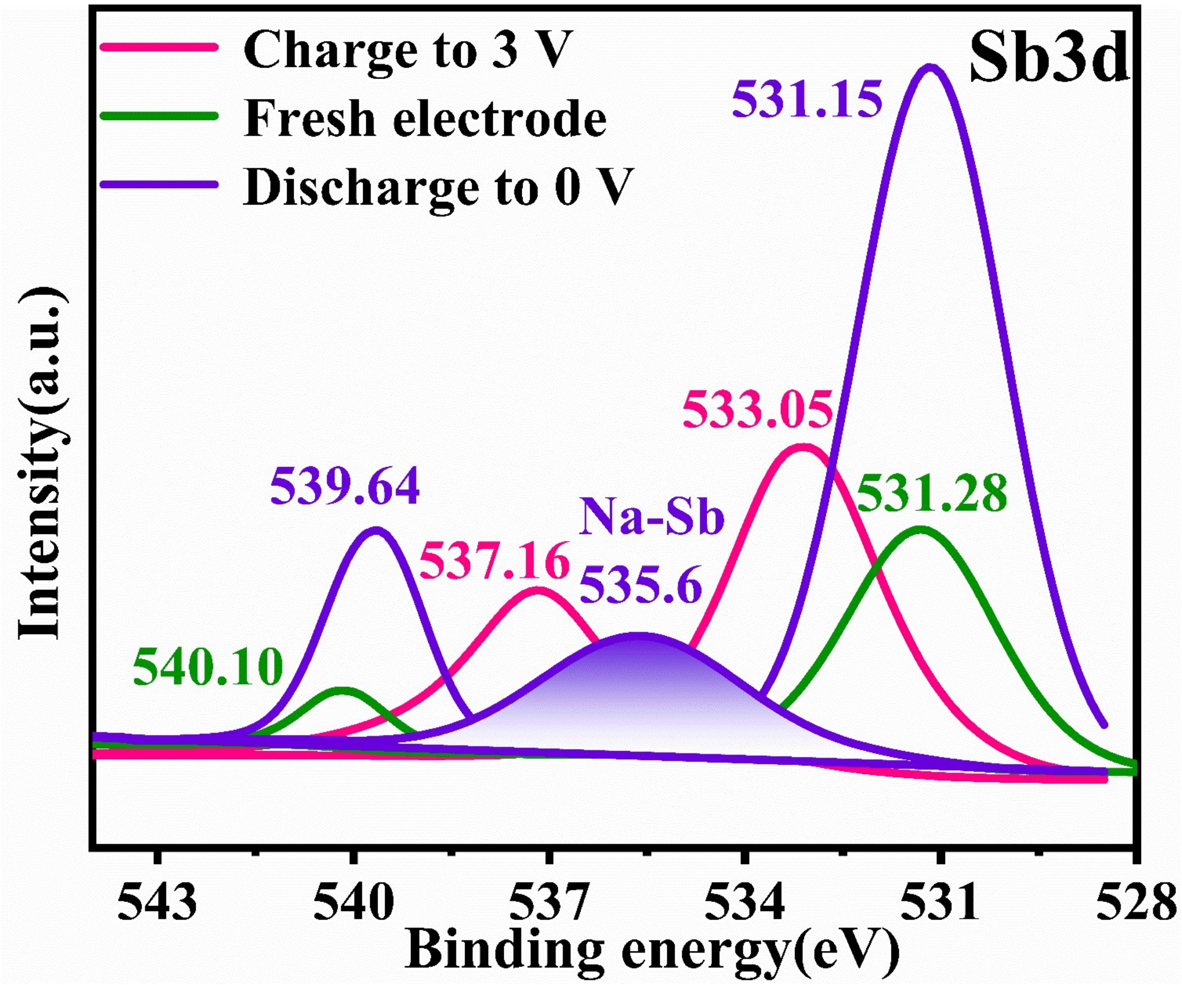

Fig. S6. Presents the *ex*-situ Sb 3d XPS spectra of the FeSb/FeS-G electrode at discharged (0 V) and charged (3 V) states, compared with that of the pristine electrode.

To further investigate the discharge/charge products, *ex*-situ TEM, SAED, and EDS analyses were carried out on the FeSb/FeS-G electrode after five cycles at a current density of 0.2 A/g, discharged to 0 V and charged to 3 V, respectively. Figures S7a–c and S7d–f show the morphology, TEM, and SAED images of the FeSb/FeS-G electrode after discharge to 0 V and charge to 3 V, respectively. Small nanoparticles with diameters ranging from 10 to 200 nm can be clearly observed on the electrode surface. These discharge/charge products are uniformly anchored onto exfoliated graphite nanosheets (Figures S7a, S7d). Figures S7b and S7e are enlarged TEM images from the blue-circled areas of Figures S7a and S7d, respectively, while Figures S7c and S7f correspond to the yellow-circled regions. After discharge to 0 V, the presence of Na_2S, Na_3Sb, and Fe was detected (Figure S7b), whereas FeSb and FeS phases were identified after charging to 3 V (Figure S7e). Furthermore, the diffraction spots observed in the SAED patterns (Figures S8c and S8f) confirm the presence of these phases, providing strong evidence for the full reversibility of FeS and the partial reversibility of FeSb.

These TEM observations are in good agreement with the proposed electrochemical reaction mechanism, further validating the charge/discharge pathway of the composite. Figures S7g and g_1–g_5, as well as S7h and h_1–h_5, present the elemental mapping of the FeSb/FeS-G electrode after discharge to 0 V and charge to 3 V, respectively, showing highly uniform elemental distributions. This indicates good dispersion of the components, which facilitates Na^+ diffusion. Figures S7i and S7j show the EDS spectra of the FeSb/FeS-G electrode after discharge to 0 V and charge to 3 V, respectively.

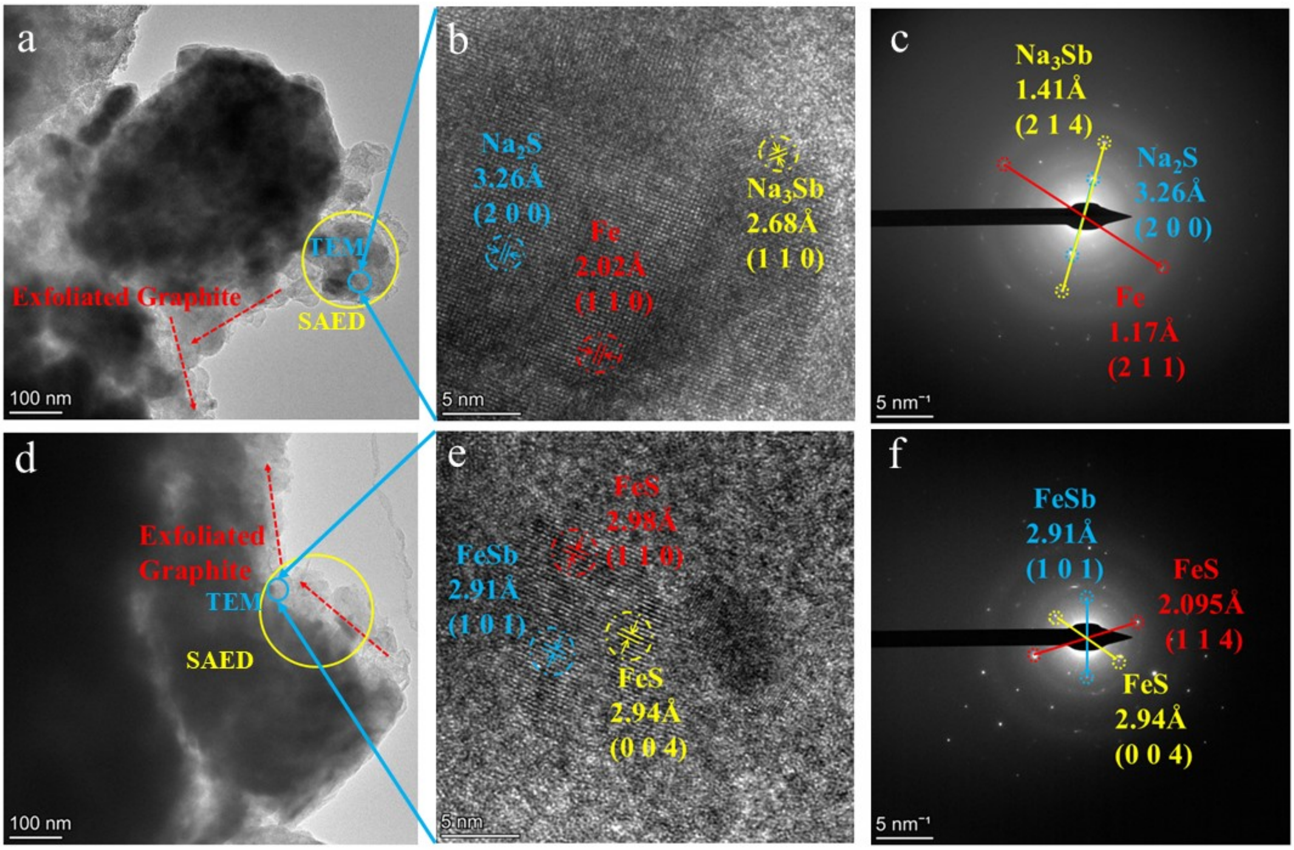

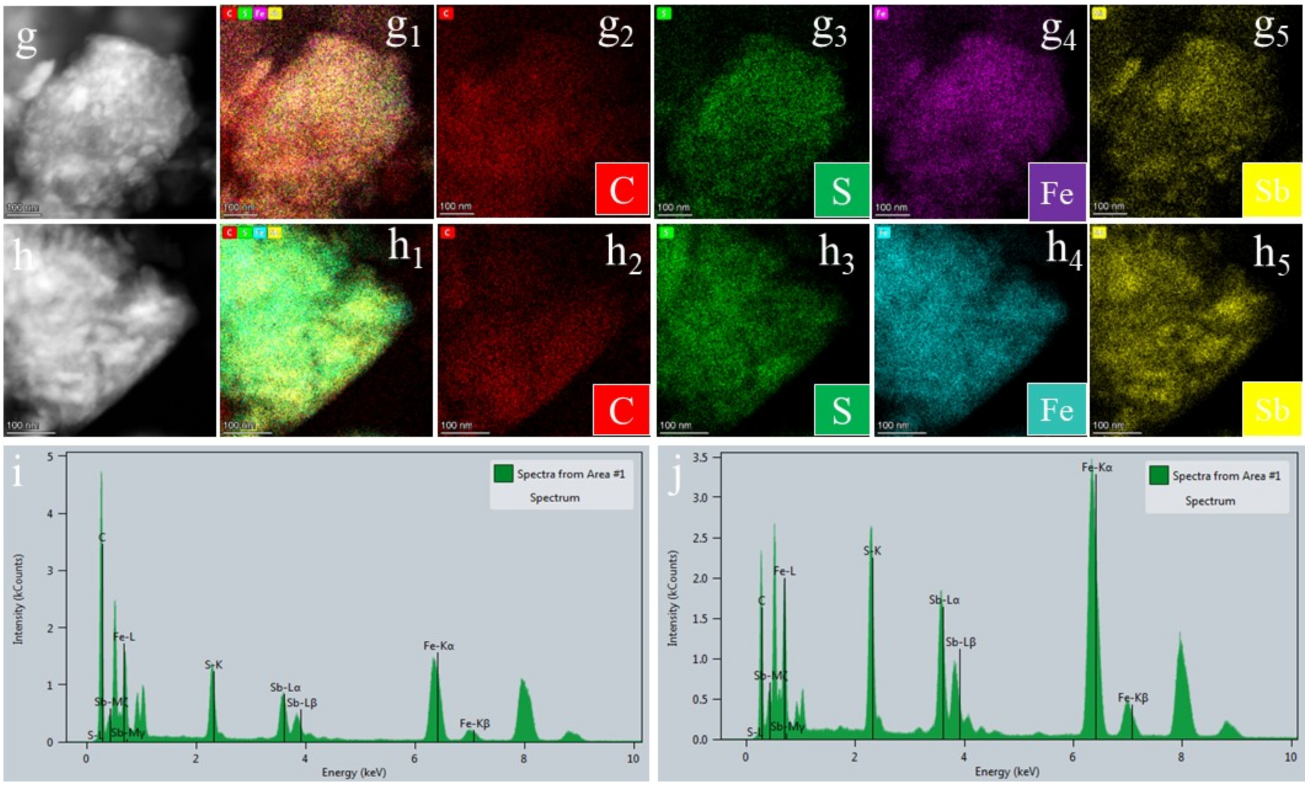

Fig. S7. (a–c) and (d–f) show the morphology, TEM, and SAED images of the FeSb/FeS-G electrode after discharge to 0 V and charge to 3 V, respectively. (g, g1–g5) and (h, h1–h5) present the corresponding elemental mapping images after discharge to 0 V and charge to 3 V. (i, j) display the EDS spectra of the FeSb/FeS-G electrode under the same discharge/charge states.

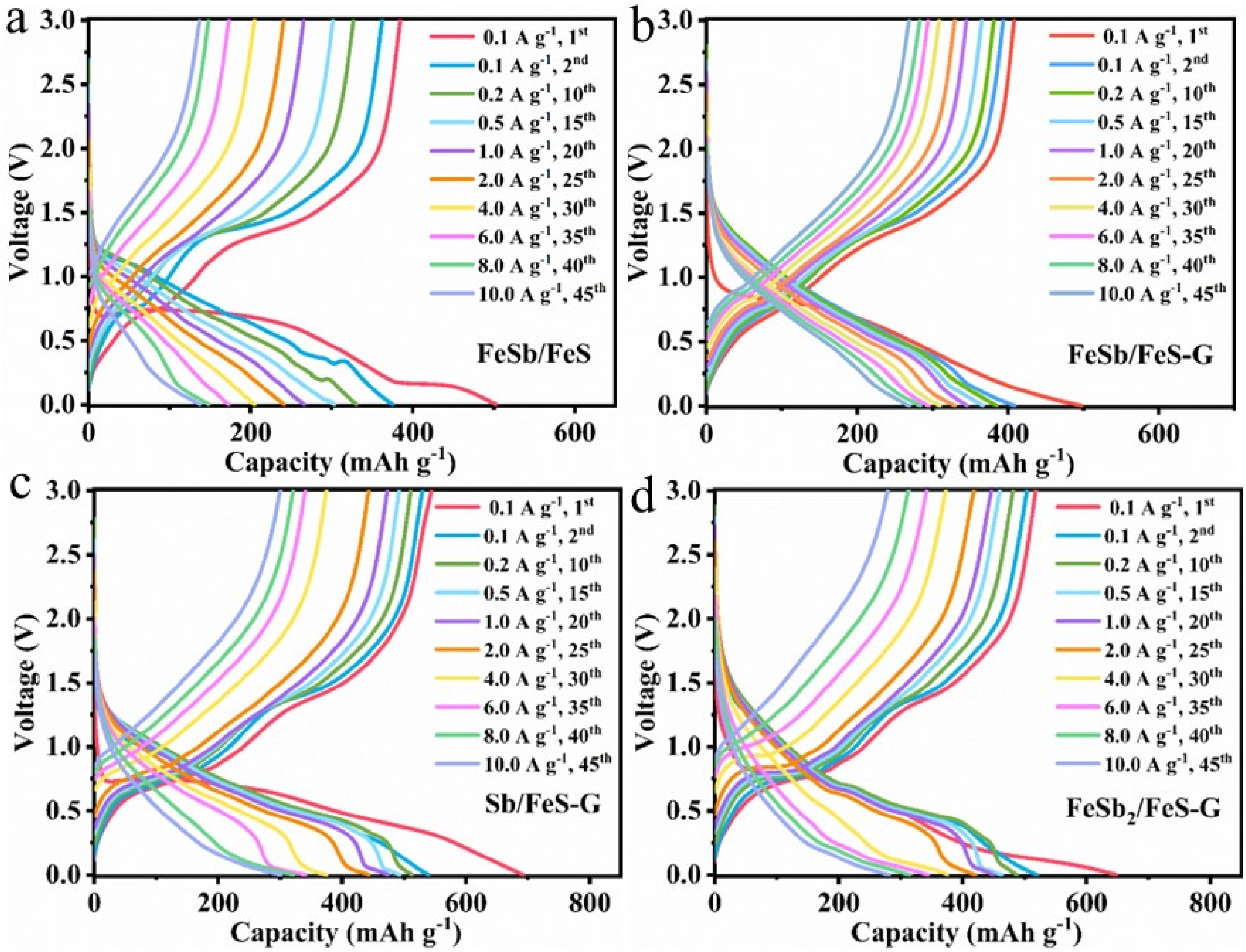

Fig. S8. (a-d) Rate capability charge-discharge curves of FeSb/FeS、FeSb/FeS-G、Sb/FeS-G和FeSb$_2$/FeS-G.

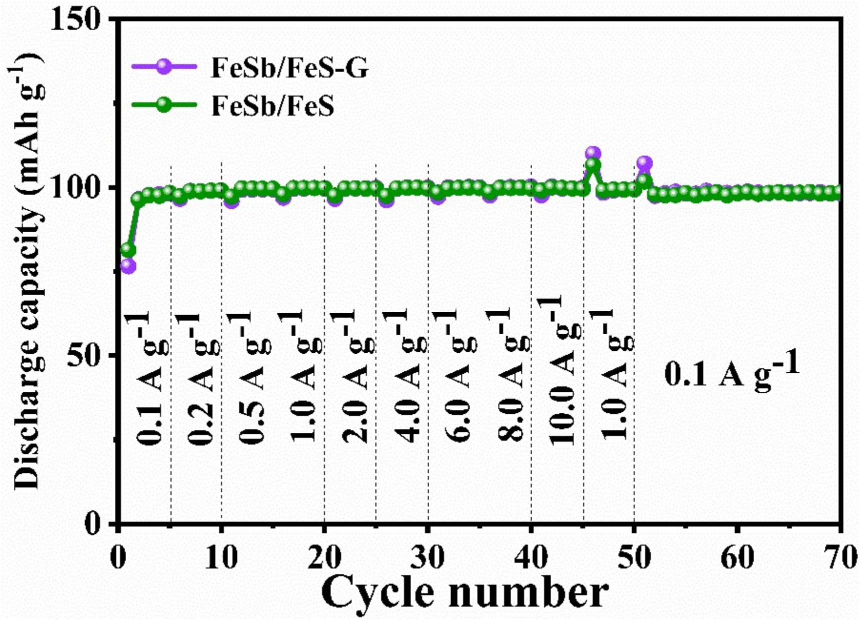

Fig. S9. Coulombic efficiency of FeSb/FeS and FeSb/FeS-G at current densities ranging from 0.1 to 10 A/g.

Since the referenced literature does not provide the specific theoretical capacity of the corresponding materials and it cannot be directly calculated, a comparison based on rate performance curves is adopted instead.

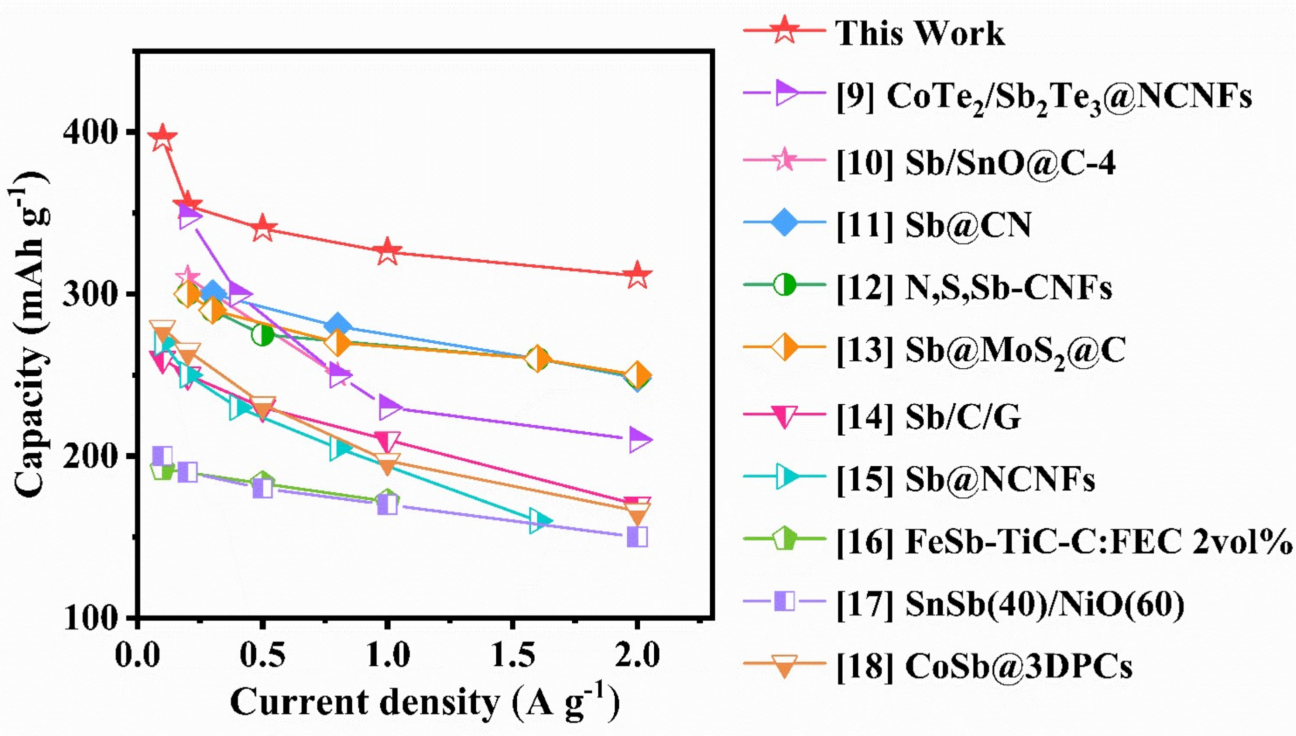

Fig. S10. Comparison of rate performance with previously reported materials.[9-18]

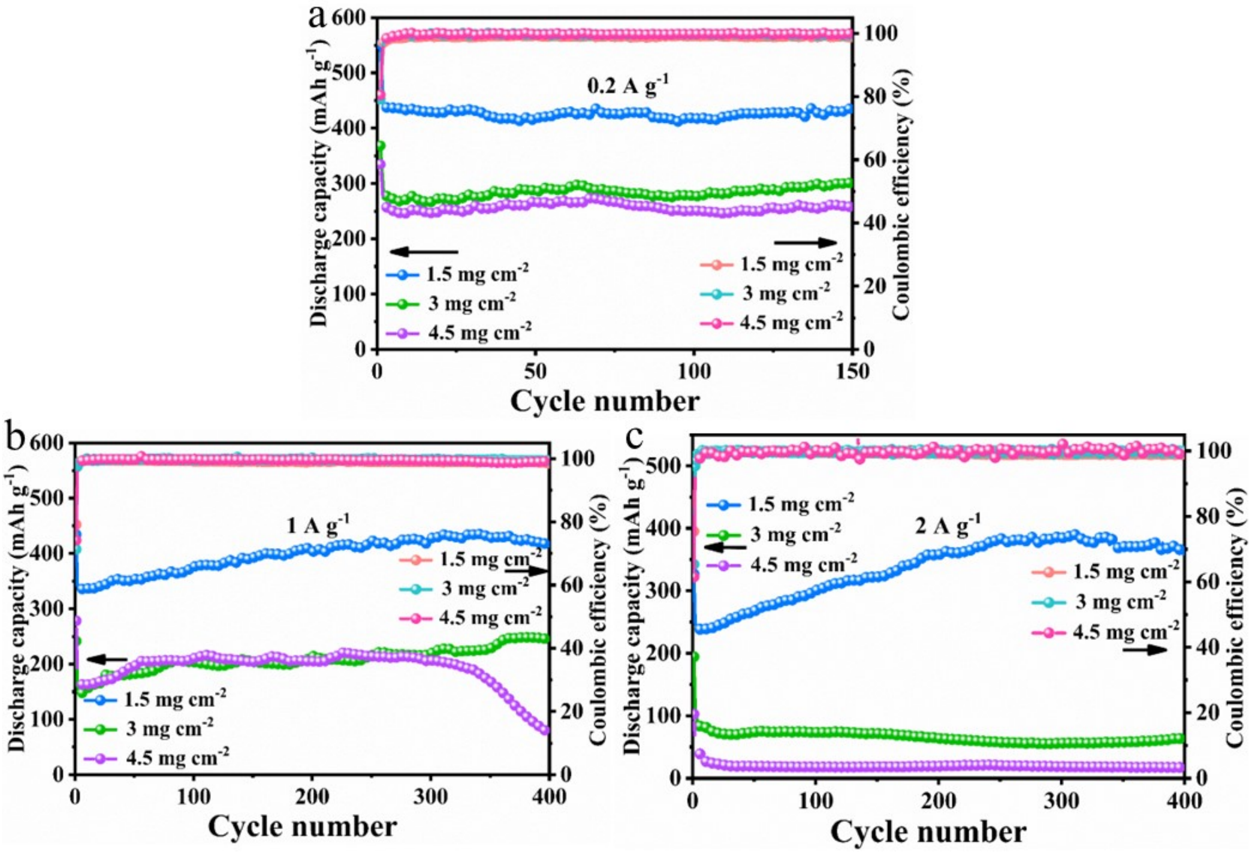

Fig. S11. Comparison of the electrochemical performance of FeSb/FeS-G electrodes with different mass loadings at current densities of 0.2 A/g, 1 A/g, and 2 A/g.

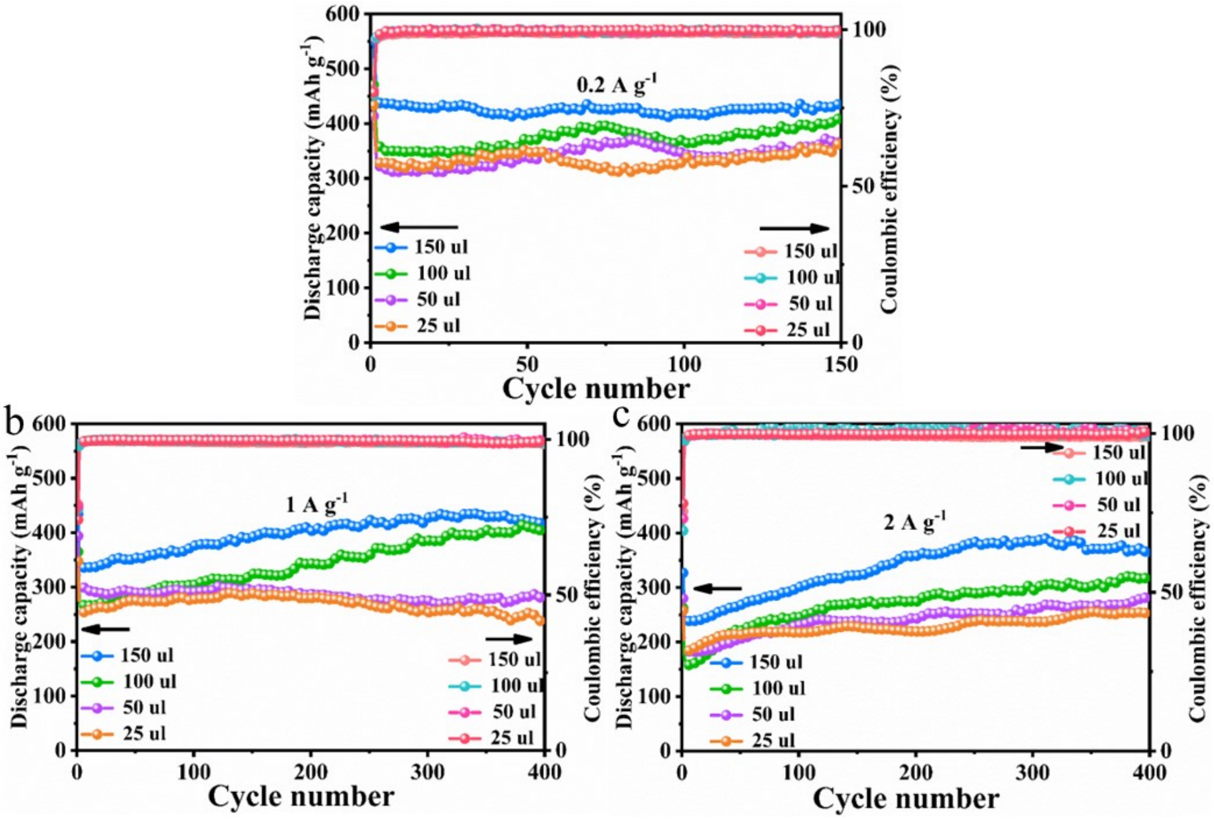

Fig. S12. Comparison of the electrochemical performance of FeSb/FeS-G electrodes with different electrolyte volumes at current densities of 0.2 A/g, 1 A/g, and 2 A/g.

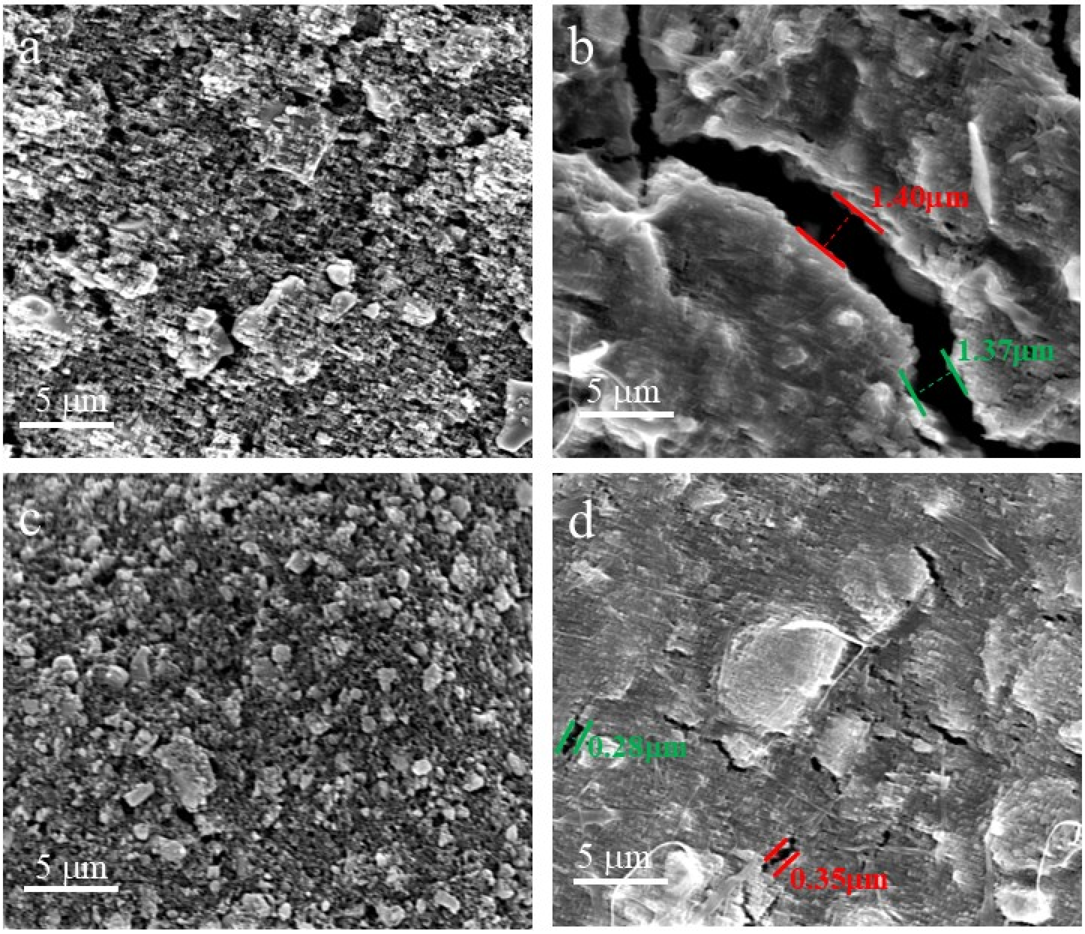

Fig. S13. (a,c) SEM scans of FeSb/FeS and FeSb/FeS-G pristine poles, respectively, and (b,d) SEM scans of FeSb/FeS and FeSb/FeS-G poles, after cell removal at 6 A/g for 900 cycles.

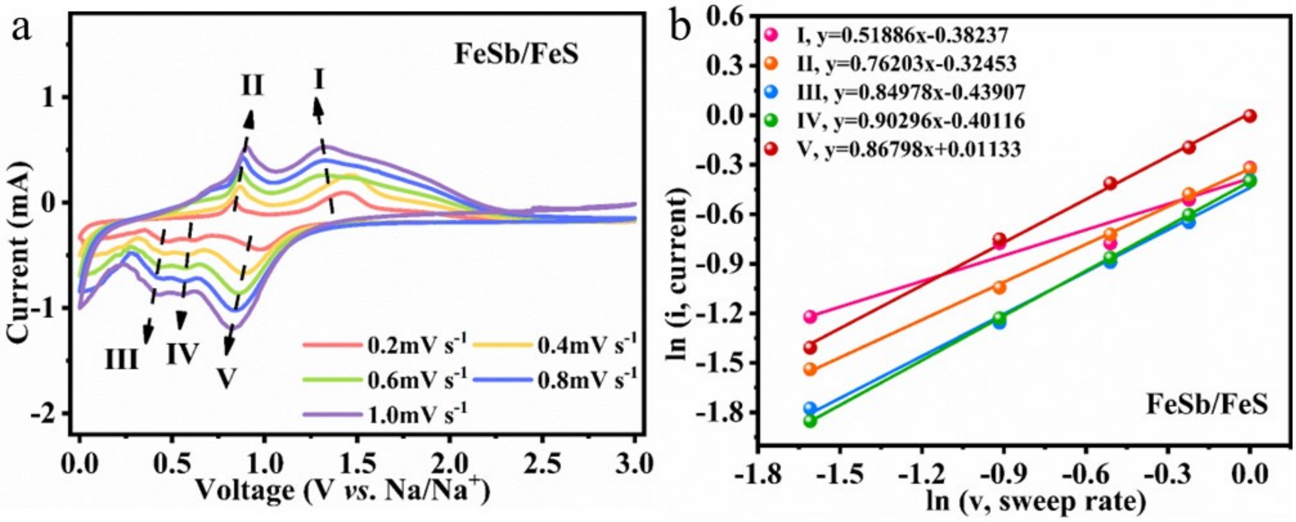

Fig. S14. (a) Re-measured CV curves of FeSb/FeS at different scan rates. (b) Relationship between peak current and scan rate for FeSb/FeS.

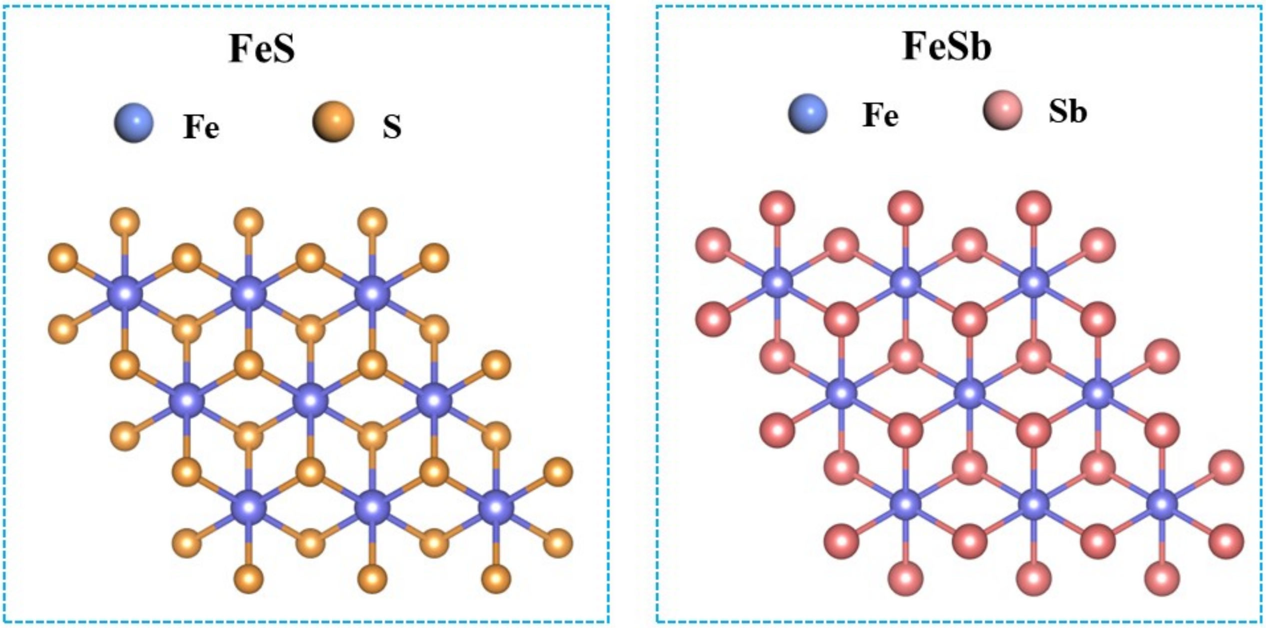

Fig. S15. (a) Crystal structure of FeS, (b) Crystal structure of FeSb.

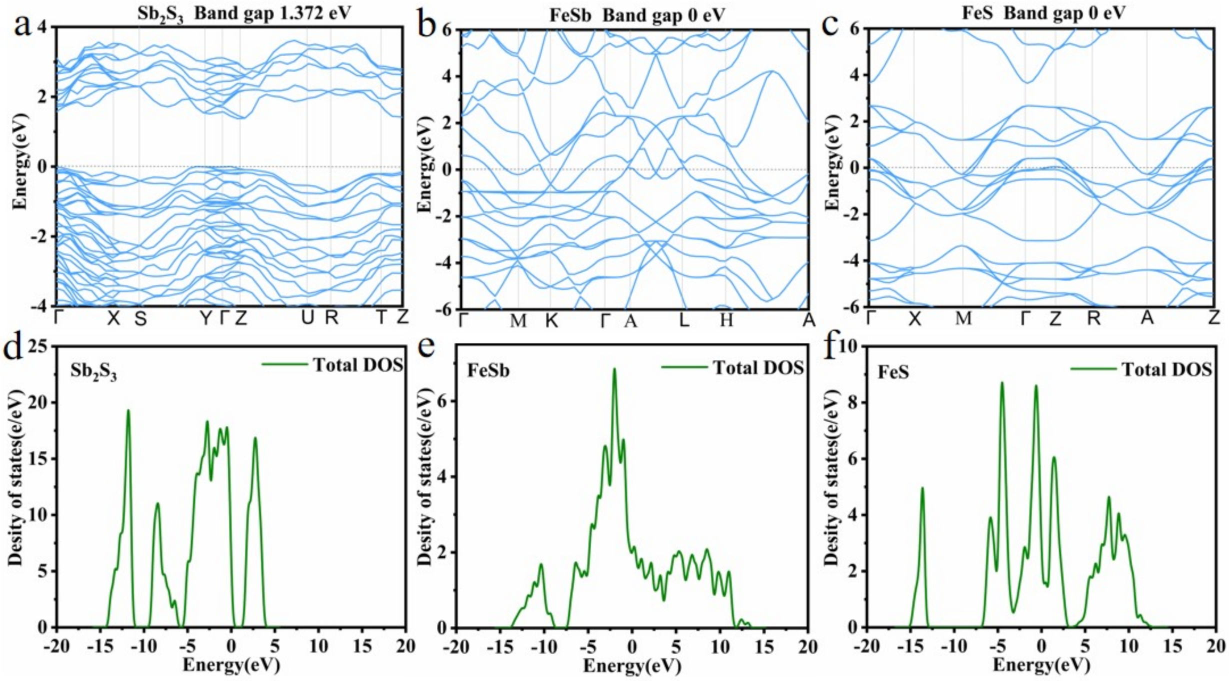

Fig. S16. (a) Energy band structure of Sb_2S_3, (b) Energy band structure of FeSb, (c) Energy band structure of FeS, (d) DOS map of Sb_2S_3, (e) DOS map of FeSb, (f) DOS map of FeS.

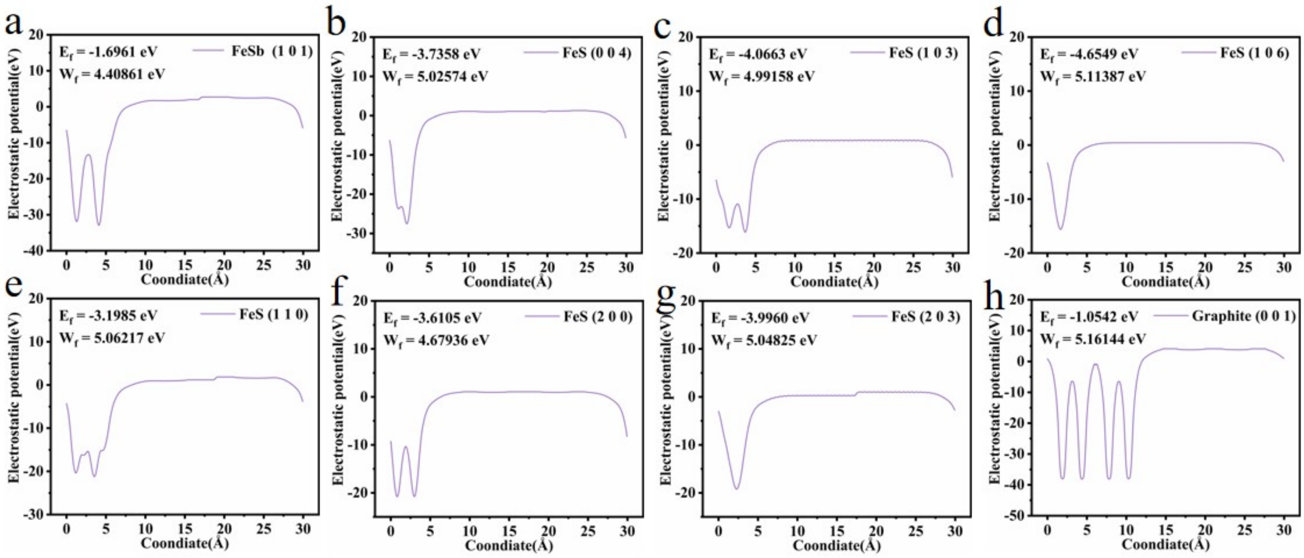

Fig. S17. Work functions for FeSb, FeS and graphite. (a) FeSb (1 0 1) plane, (b) FeS (0 0 4) plane, (c) FeS (1 0 3) plane, (d) FeS (1 0 6) plane, (e) FeS (1 1 0) plane, (f) FeS (2 0 0) plane, (g) FeS (2 0 3) plane, and (h) graphite (0 0 1) plane.

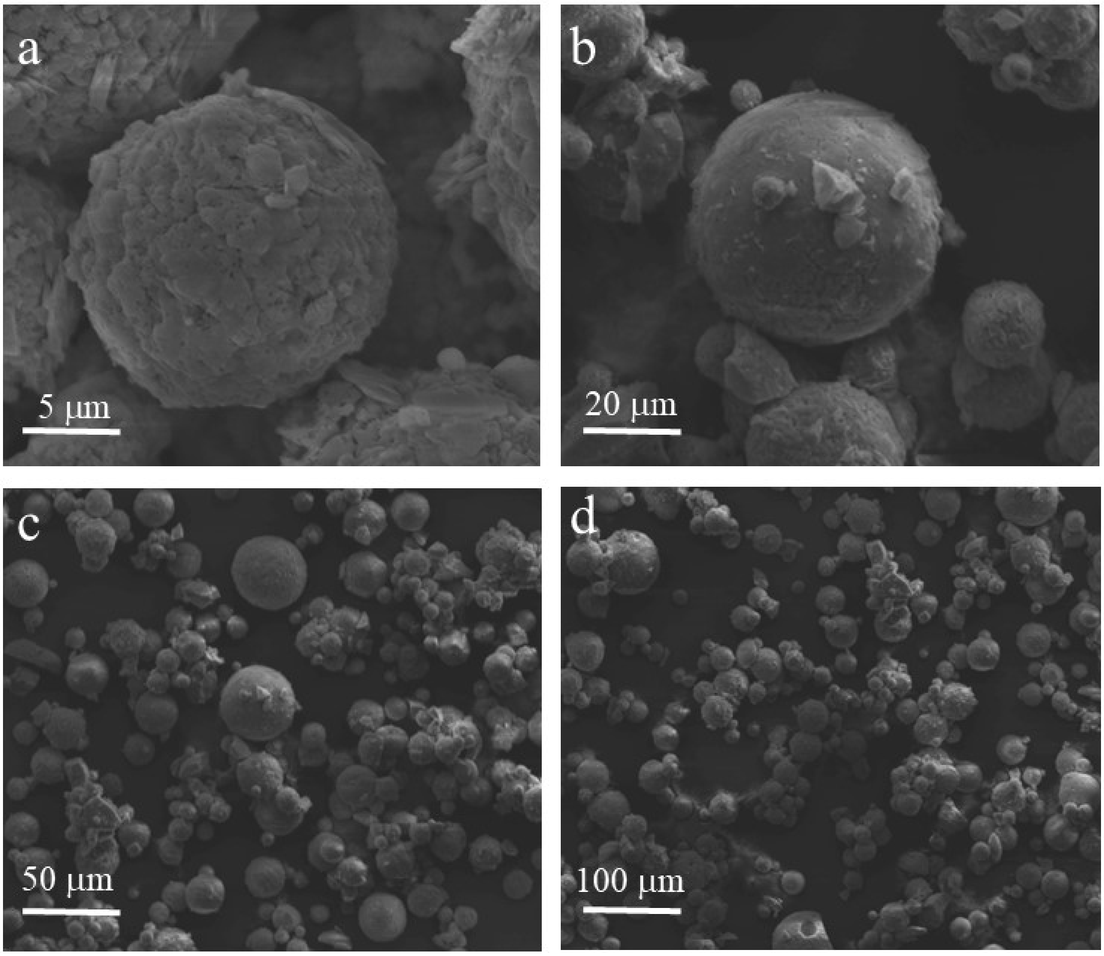

Fig. S18. (a-d) SEM images of $Na_3V_2(PO_4)_3$ at magnifications of 20,000 X, 4,000 X, 1,200 X, and 1,000 X, respectively.

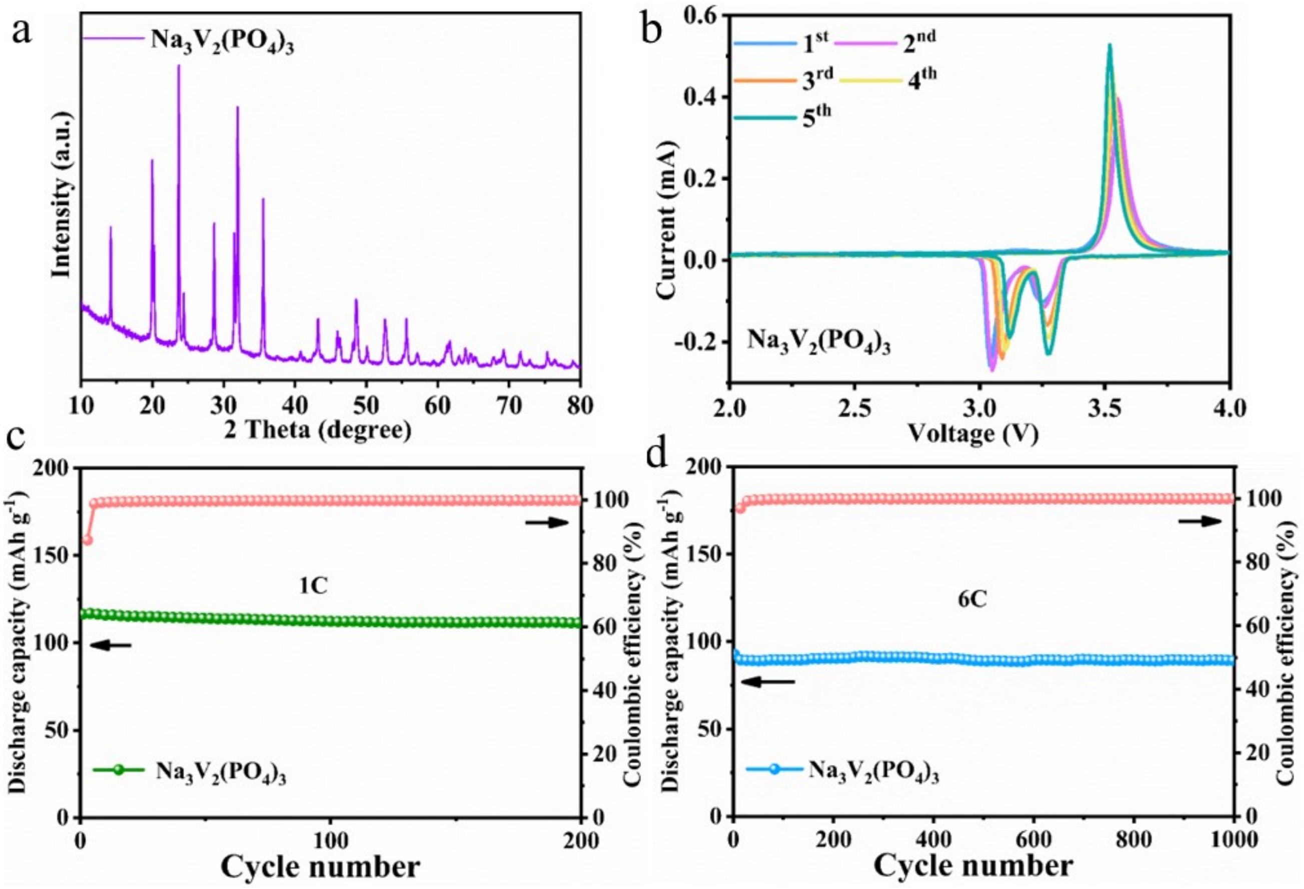

Fig. S19. (a) XRD pattern of $Na_3V_2(PO_4)_3$ and the standard PDF (JCPDS #00-53-0018),[19] (b) CV image of $Na_3V_2(PO_4)_3$, (c,d) Cycling performance of $Na_3V_2(PO_4)_3$ at current densities of 1C and 6C, respectively.

References

1. **H. Tian, Z. Xu, K. Liu, D. Wang, L. Ren, Y. Wei, L. Chen, Y. Chen, S. Liu and H. Yang, Heterogeneous bimetallic selenides encapsulated within graphene aerogel as advanced anodes for sodium ion batteries, *J. Colloid Interface Sci.*, 2024, 670, 152-162.**
2. **C. Costentin and J.-M. Savéant, Energy storage: pseudocapacitance in prospect, *Chemical Science*, 2019, 10, 5656-5666.**
3. **Y. Jiang and J. Liu, Definitions of Pseudocapacitive Materials: A Brief Review, *ENERGY & ENVIRONMENTAL MATERIALS*, 2019, 2, 30-37.**
4. **D. W. Dees, S. Kawauchi, D. P. Abraham and J. Prakash, Analysis of the Galvanostatic Intermittent Titration Technique (GITT) as applied to a lithium-ion porous electrode, *J. Power Sources*, 2009, 189, 263-268.**
5. **W. Weppner and R. A. Huggins, Determination of the Kinetic Parameters of Mixed-Conducting Electrodes and Application to the System Li3Sb, *J. Electrochem. Soc.*, 1977, 124, 1569.**
6. **D. J. Brooks, B. V. Merinov, W. A. Goddard, III, B. Kozinsky and J. Mailoa, Atomistic Description of Ionic Diffusion in PEO–LiTFSI: Effect of Temperature, Molecular Weight, and Ionic Concentration, *Macromolecules*, 2018, 51, 8987-8995.**
7. **A. Ghysels, R. M. Venable, R. W. Pastor and G. Hummer, Position-Dependent Diffusion Tensors in Anisotropic Media from Simulation: Oxygen Transport in and through Membranes, *J. Chem. Theory Comput*, 2017, 13, 2962-2976.**
8. **X. Ding, W. Yuan, Y. Fan, Y. Chen, Y. Yang, L. Liu and L. Han, Tremendously excess Na-storage capacity of Sb@C anode towards high-performance sodium-ion batteries, *Chem. Eng. J.*, 2025, 505, 159402.**
9. **W. Fan, J. Huang, W. Zhang, W. Zhao, L. Wang, J. Wu, G. Wang and S. Huang, Synergistic effects of confined substitution and architecture engineering in CoTe2/Sb2Te3 heterostructures towards durable and fast sodium storage, *Mater. Today Phys*, 2024, 41, 101342.**
10. **W. Yao, J. Zhao, Q. Li, C. Yu and X. Ding, Sb/SnO@C composite prepared by electrospinning for high performance sodium ion battery anodes, *J. Phys. Chem. Solids*, 2023, 183, 111647.**
11. **Q. Mao, Y. Jia, W. Zhu and L. Gao, Stable sodium-ion battery anode enabled by encapsulating Sb nanoparticles in spherical carbon shells, *J. Solid State Electrochem.*, 2023, 27, 1433-1441.**
12. **J. You, H. Sun, X. Wang, M. Li, J. Sun, P. Wang, Y. He and Z. Liu, Sb Ultra-Small Nanoparticles Embedded within N, S co-Doped Flexible Carbon Nanofiber Films with Longitudinal Tunnels as High Performance Anode Materials for Sodium-Ion Batteries, *Batteries & Supercaps*, 2023, 6, e202300022.**
13. **Z. Li, X. Wang and Y. Wang, Encapsulating Sb/MoS2 Into Carbon Nanofibers Via Electrospinning Towards Enhanced Sodium Storage, *ChemistrySelect*, 2024, 9, e202400172.**
14. **H.-J. Li, J.-J. Li, Z. Chen, Z.-Z. Wang, J. Qu, Y.-Q. Chen, L.-J. Zhu and F. Jiang, Blocky Sb/C Anodes with Enhanced Diffusion Kinetics for High-Rate and Ultra-Long Cyclability Sodium Dual-Ion Batteries, *ChemElectroChem*, 2021, 8, 3512-3518.**
15. **L. Yang, B. Yang, X. Chen, H. Wang, J. Dang and X. Liu, Bimetallic alloy SbSn nanodots filled in electrospun N-doped carbon fibers for high performance Na-ion battery anode, *Electrochim. Acta*, 2021, 389, 138246.**

16. I. T. Kim, E. Allcorn and A. Manthiram, High-performance FeSb–TiC–C nanocomposite anodes for sodium-ion batteries, *PCCP*, 2014, 16, 12884-12889.

17. A. Verdianto, H. Lim, J. G. Kang and S.-O. Kim, Scalable, colloidal synthesis of SnSb nanoalloy-decorated mesoporous 3D NiO microspheres as a sodium-ion battery anode, *Int. J. Energy Res*, 2022, 46, 4267-4278.

18. D. Wang, Q. Ma, K. Tian, Z. Wang, H. Sun and Y. Liu, Nanosized CoSb Alloy Confined in Honeycomb Carbon Framework Toward High-Property Potassium-Ion and Sodium-Ion Batteries, *Energy Technol*, 2021, 9, 2100095.

19. Y. Liu, X. Wu, A. Moeez, Z. Peng, Y. Xia, D. Zhao, J. Liu and W. Li, Na-Rich Na3V2(PO4)3 Cathodes for Long Cycling Rechargeable Sodium Full Cells, *Adv. Energy Mater*, 2023, 13, 2203283.